Solid Freeform Fabrication 2017: Proceedings of the 28th Annual International Solid Freeform Fabrication Symposium – An Additive Manufacturing Conference
Reviewed Paper

FLEXURAL BEHAVIOR OF FDM PARTS: EXPERIMENTAL, ANALYTICAL AND NUMERICAL STUDY

Madhukar Somireddy*[1], Diego A. de Moraes*, and Aleksander Czekanski*
*Department of Mechanical Engineering, York University, Toronto, ON, M3J 1L4, Canada
[1]Corresponding author: madhukar@yorku.ca

Abstract

Fused deposition modelling (FDM) processed parts behave as composite laminate structures. Therefore, mechanics of composite laminates can be adopted for the characterization of mechanical behavior of the printed parts. In this study, the flexural properties of the 3D printed laminates are investigated experimentally, analytically and numerically. Each layer of the printed specimens is treated as an orthotropic material. The elastic moduli of a lamina are calculated by considering the mesostructure of the printed laminate in finite element simulation of tensile testing. These elastic moduli are employed in a constitutive matrix for the calculation of flexural stiffness of the laminate using classical laminate theory. Then 3-point bending tests are conducted on the printed laminates to calculate their flexural stiffness. The influence of road/ fiber size and lamina layup on the flexural properties are also investigated. Furthermore, failure phenomena of printed laminates under bending loads is investigated.

Introduction

In recent times additive manufacturing (AM) techniques have risen in popularity [1] and these techniques have broad applications in the field of mechanical, aerospace and biomedical engineering [2]. AM techniques lack the limitations on fabricating parts with complex geometry in contrast to subtractive or conventional machining processes. However, the maximum size of the part remains a limiting factor when building using these advanced fabrication methods at present. The metal additive manufacturing industry has already found a way in the mass production of jet engines parts [4]. In near future, these AM processes will responsible for a major change in the design of materials as well as components. Traditionally, parts have been designed with manufacturability being a major consideration. Because of the limitation on complexity, the geometry of constructed parts was limited to what was reproducible using traditional manufacturing methods. Modern AM techniques allow for manufacturers to tailor the material properties by designing the microstructure of a material. The material properties of the final printed part differ from initial material properties. The change in the mechanical properties of a material of the printed parts is addressed in [5]. The difference in the material properties is due to changes in the microstructure of a material that is taking place during layer by layer printing while building a 3D part. The variation in the mechanical properties should be taken into consideration when measuring the final properties, which are useful in the design and analysis of the parts.

Fused deposition modeling is an AM technique, in which a 3D part is fabricated by deposition of material one layer at a time. FDM is one of the most popular and widely used processes among all additive manufacturing techniques for 3D printing of parts. In the FDM process, hot molten filament material is extruded from the nozzle and deposited on a bed. The filament on the bed is referred to as the road. Subsequent roads are deposited side by side and will have a bond with previously deposited road to form a single layer, then the next layer is deposited on the previous layer to build a 3D part. Each layer in a printed part behaves as an orthotropic material even though the initially filament material is isotropic [7]. The layers can be treated as a unidirectional fiber reinforced lamina in laminated composite structure. This means, the roads in a layer act as fibers in a lamina and several layers together with different printing orientations behave as laminated composite structures [16]. Therefore, parts printed via FDM can be considered laminated composites for the purposes of the characterization of their mechanical behavior. In this paper, the mechanical behavior of the printed laminated parts under bending load is investigated. Researchers [6-8] have been working towards the characterization of mechanical behavior of printed parts. It is revealed that the process parameters of the FDM process influence the mechanical properties by researchers [9-11] and further these are cause for introducing anisotropy in the printed part. The effect of different process parameters such as printing direction, layer thickness, gap between the adjacent fibers on the mechanical properties is investigated by [12]. It is found that the printing direction has a profound effect on the final properties of the printed part. The printing chamber temperature influences the bonding strength between adjacent fibers in

the part while printing [13-15]. Additionally, the boding strength between the roads has an effect on the final properties of the part. Kulkarni and Dutta [16] adopted the laminate theory for the characterization of FDM printed parts and then researchers [17,18] further worked on implementing the CLT for the FDM parts. The mesostructure of FDM printed parts influences the mechanical properties of the part. Alaimo et al. [19] carried-out experimental investigation to study the influence of the mesostructure and the composition of the filament on the mechanical properties on FDM printed parts. Furthermore, the CLT and laminate failure theory was adopted for studying the mechanical behavior of the printed parts. The filament material used in FDM process for printing parts is typically plastic; mainly PLA and ABS. Since the plastic material does not have better mechanical properties when compared to metals, researchers are working to improve the properties of FDM printed parts by adding reinforcements in the plastic filament material [20]. Composite filaments using carbon nanotubes as additional reinforcements in the thermoplastic materials have been developed [21,22] for better mechanical and electrical properties. These composite filament materials are broadening industrial applications of FDM processes, increasing adoption in for example biomedical industries [3].

The FDM printed parts behave in an anisotropic nature, therefore the failure in such parts is complex. Failure phenomena of FDM printed parts under tensile, compressive and bending loads should be investigated. Ziemian et al. [23] studied influence of printing direction/raster orientation on the mechanical properties and conducted failure analysis of FDM printed parts under tensile, compressive, flexural and impact loads. Furthermore, damage analysis of FDM printed parts under fatigue load is investigated in [24]. Hart and Wetzel [25] studied the fracture behavior of the fused deposited parts, where brittle behavior and ductile response were observed. They found that the facture behavior depends on the lamina orientation.

The present paper mainly focuses on the flexural behavior of the laminates fabricated via fused deposited modeling. The elastic moduli in stiffness matrix of printed lamina are calculated by accounting the mesostructure of the FDM processed laminates in the finite element models. For this, three different types of FE models are developed and simulated to find the elastic moduli. Then the elastic moduli of lamina are used in the classical laminate theory flexural behavioral characterization of the laminates. Also, flexural stiffness of the laminates is calculated for four different lamina layups. Then the 3-point bending tests are conducted on the printed laminate to find the flexural stiffness of the laminates. The stiffness values obtained from experiments are validated with analytical results obtained using CLT. Furthermore, the failure surface of cross ply laminates is characterized. Failure modes happened under bending loads that are discussed.

Methodology

Parts printed via FDM resemble unidirectional fiber reinforced laminated composite structures, therefore mechanics of laminated composites are adopted for the analysis of the printed laminates. The behavior of printed laminate with different printing direction in each layer is an anisotropic. Furthermore, the layer/lamina in the laminate behaves as an orthotropic material. The material behavior of the laminate is accounted for in the analysis by considering the constitutive matrix of the lamina in it. Therefore, the stiffness/constitutive matrix of lamina is required to find to the material behavior of the laminate in the characterization of their mechanical behavior. This section initially describes the FE procedure to calculate the stiffness matrix of lamina. The stiffness matrix is calculated from FE simulations. Then the following sections after that explain analytical flexural behavior characterization of the printed laminates using classical laminate theory and finally experimental characterization is done.

Constitutive matrix of a lamina: Numerical

The FDM process fabricates the parts by layer upon layer deposition of material, each layer acts a unidirectional fiber reinforced lamina. The lamina is a thin layer and therefore it can be treated as plane stress case. The strain-stress relation for the lamina for a plane stress case is written as

$$\begin{Bmatrix} \varepsilon_{11} \\ \varepsilon_{22} \\ \gamma_{12} \end{Bmatrix} = \begin{bmatrix} S_{11} & S_{12} & 0 \\ S_{12} & S_{22} & 0 \\ 0 & 0 & S_{66} \end{bmatrix} \begin{Bmatrix} \sigma_{11} \\ \sigma_{22} \\ \tau_{12} \end{Bmatrix} \tag{1}$$

Numerical suffix denotes coordinate system, 1 is along the fiber and 2 is across the fiber orientation. The coefficients of compliance matrix ***S*** are available in Eq.2.

$$S_{11} = \frac{1}{E_1}, S_{12} = -\frac{\nu_{12}}{E_2}, S_{22} = \frac{1}{E_2}, S_{66} = \frac{1}{G_{12}} \tag{2}$$

The plane stress reduced constitutive relation for an orthotropic material is obtained by inverting Eq.1

$$\begin{Bmatrix} \sigma_{11} \\ \sigma_{22} \\ \tau_{12} \end{Bmatrix} = \begin{bmatrix} Q_{11} & Q_{12} & 0 \\ Q_{12} & Q_{22} & 0 \\ 0 & 0 & Q_{66} \end{bmatrix} \begin{Bmatrix} \varepsilon_{11} \\ \varepsilon_{22} \\ \gamma_{12} \end{Bmatrix} \tag{3}$$

where the Q_{ij} are coefficients of the plane stress reduced stiffness matrix ***Q***, and given by

$$\begin{aligned} Q_{11} &= \frac{S_{22}}{S_{11}S_{22} - S_{12}^2} = \frac{E_1}{1-\nu_{12}\nu_{21}}, Q_{12} = \frac{S_{12}}{S_{11}S_{22} - S_{12}^2} = \frac{\nu_{12}E_1}{1-\nu_{12}\nu_{21}} \\ Q_{22} &= \frac{S_{11}}{S_{11}S_{22} - S_{12}^2} = \frac{E_2}{1-\nu_{12}\nu_{21}}, Q_{66} = \frac{1}{S_{66}} = G_{12} \end{aligned} \tag{4}$$

Note that the reduced stiffness matrix's components involve only four independent material constants, E_1, E_2, ν_{12} and G_{12} . That means the number of elastic constants of orthotropic material for a plane stress case reduced to four. These elastic constants are required to characterize the mechanical behavior of the FDM processed parts, which resemble laminates. These unknown constants can be obtained by conducting finite element simulation on three different tensile test specimens, explained below. All tensile test specimens considered in this paper follow standards mentioned earlier and elasto-static analysis is carried-out initially on these specimens using the finite element method.

Let us consider a first case, where the fiber (road) is oriented along the axis of the loading in test specimen. The test specimen is subjected to uniaxial tensile loading, as shown in Fig. 1*a*. The elastic modulus E_1 and ν_{12} of lamina can be calculated from this case. For a uniaxial tensile testing case, using stress-strain relation and strain-displacement relation, the strain energy is written as

$$U = \frac{1}{2} E_1 \left(\frac{\delta l}{l} \right)^2 V \tag{5}$$

The fiber orientation and type of loading in this case is replicated in the finite element model of the tensile test specimen after which the simulation is carried out. The strain energy (*U*) and displacement δl along the axis of the load are obtained from finite element simulation. The length between grips *l* and volume of member that undergone deformation *V* are given. The only unknown, E_1 is calculated from Eq. 5. The Poisson's ratio given as $\nu_{12} = -\varepsilon_{22}/\varepsilon_{11}$, where ε_{22} is lateral strain. The lateral strain is calculated by later displacement upon the original width in gage area of tensile member.

Now a second case, where the fiber is oriented across the axis of loading in the test specimen and is subjected to uniaxial tensile load as shown in Fig. 1*b*. From this test the unknown elastic modulus E_2 of the lamina is calculated. The total strain energy in this case is given as

$$U = \frac{1}{2} E_2 \left(\frac{\delta l}{l} \right)^2 V \tag{6}$$

Let us take a case where the fiber is oriented off axis at 45° to the axis of loading in the tensile test specimen. The uniaxial load is applied to test specimen as shown in Fig. 1*c*. This test is conducted to find the unknown shear modulus G_{12} of the lamina. The total strain energy for this case is obtained from area under stress-strain curve and is given by

$$U = \frac{1}{2} E_x \left(\frac{\delta l}{l} \right)^2 V \tag{7}$$

The fiber orientation in the tensile specimen is replicated in the FE model and the strain energy (*U*) and displacement δl along axis of the load are obtained from simulation. The unknown E_x is calculated from Eq. 7. The relation between the principal *1-2* coordinates and non-principal *x-y* coordinates established through the transformation matrix, which is useful in this case to calculate the shear modulus G_{12} and the results is given by

$$G_{12} = \frac{1}{\frac{4}{E_x} - \frac{1}{E_1} - \frac{1}{E_2} + \frac{2\nu_{12}}{E_1}} \tag{8}$$

For further details about the procedure for calculation of elastic constants of the unidirectional fiber reinforced lamina refer to [27].

Summary of linear finite element simulation procedure:

a) Develop three CAD models of the tensile test specimen with three different mesostructures (3 cases mentioned earlier, shown in Fig.1) that would be obtained from FDM process.
b) Mesh the CAD models with three dimensional finite elements.
c) Apply boundary and load conditions to simulate the tensile testing of each case.
d) Carry out the linear finite element analysis to find the strain energy and displacement that would be obtained from the simulation of each case.
e) Calculate the elastic moduli ($E_1, E_2, \nu_{12}, G_{12}$) of the lamina from three cases using Eqs. 5, 6 and 8, as explained above.

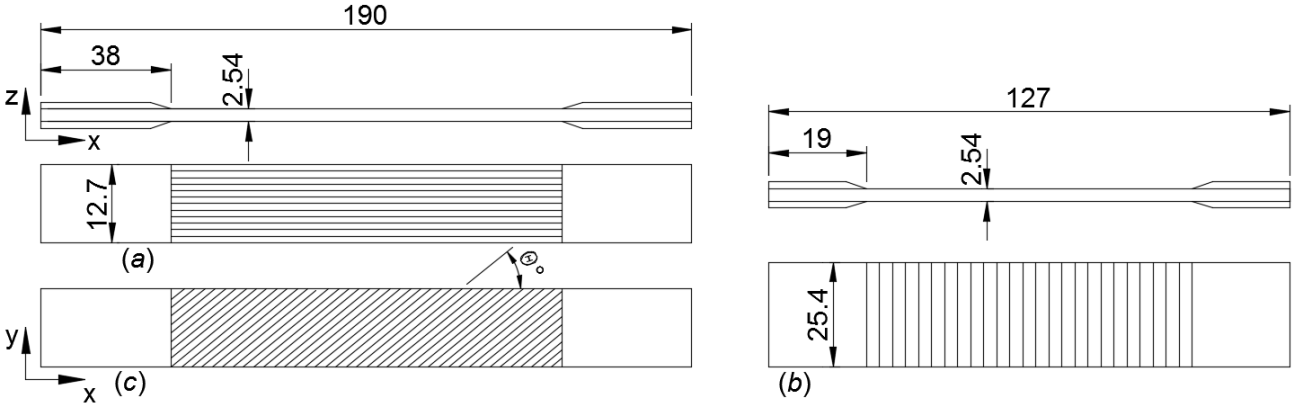

Figure 1. Dimensions of tensile specimens (*a*) fiber orientation along *x*-axis, (*b*) fiber orientation along *y*-axis, (*c*) fiber orientation 45° to *x*-axis.

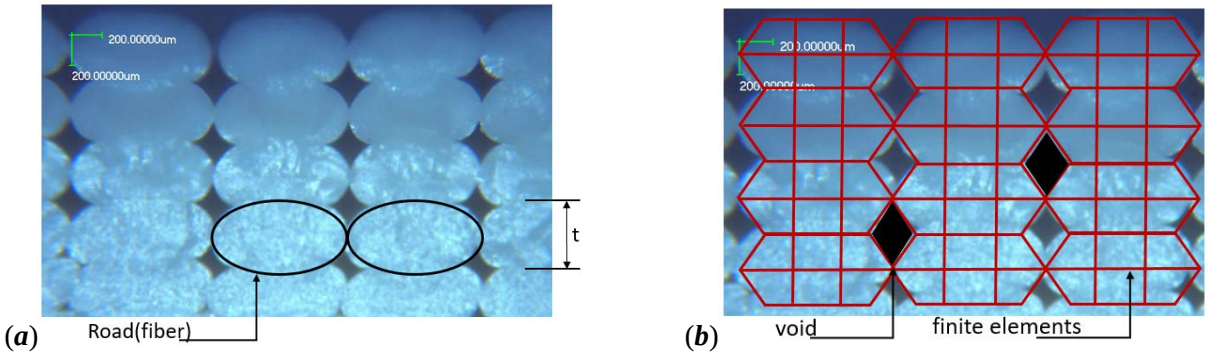

(*a*) (*b*)

Figure 2. Mesostructures (*a*) mesostructure of printed part via FDM (*b*) finite elements modeling of mesostructure

The strain energy is the energy stored by a member during the deformation and this can be calculated using finite element analysis. The calculation of strain energy of the FDM processed tensile test specimen subjected to uniaxial load is explained here and it is useful for finding the elastic constants of the layer(lamina). The uniqueness of this analysis is that the mesostructure of the material of the part that is obtained from FDM is replicated in finite element model of the tensile test specimen. This is how one can realistically simulate the FDM-processed materials to capture their mechanical behavior from the microscale level. The tensile test specimen and its cross-section with internal mesostructure obtained from 0° raster orientation to the *x*-axis in FDM are shown in Fig. 2*a*. The tensile test specimen is as per ASTM D3039 and it is subjected to uniaxial tensile loading, *P* along the *x*-axis. All dimensions of the tensile test specimen shown in Fig. 1 are in millimeters. Each road in a layer is treated as a fiber and is modeled using 3D linear finite elements as shown in Fig.2*b*. This means that the 3D constitutive relation for isotropic material is accounted in the finite element analysis. Elasto-static uniaxial tensile tests were carried out in the commercially available finite element software, Hyperworks.

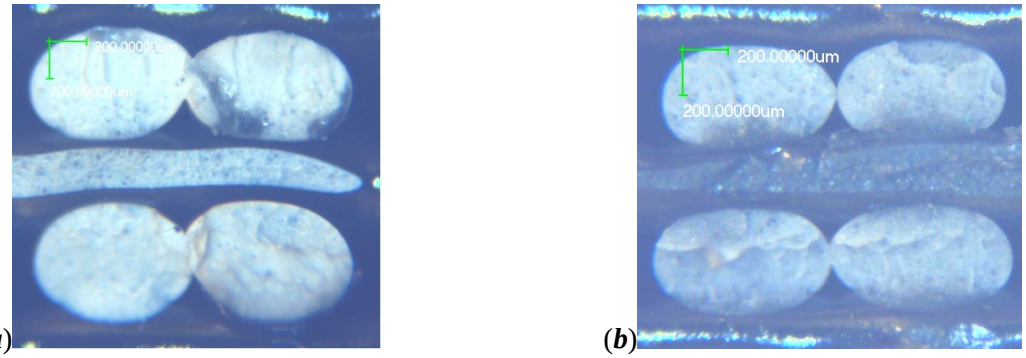

(*a*) (*b*)

Figure 3. Fiber orientation 0°/90° in a mesostructure of the printed part using FDM Stratasys µ print plus machine (*a*) 0.330 mm, (*b*) 0.254 mm layer thickness.

The mesostructure of the printed part is shown in the Fig. 2*a*. The width of the road is larger than the height of the road, the height of the road is equal to the layer thickness (*t*). The road takes on an elliptical cross section during deposition and solidification of the material [17,26]. The dimension of cross section of the road is equal to the layer height and its major axis is double the layer height. Let us consider an example mesostructure with a layer height of 0.330mm. This mesostructure is replicated in the FE models of tensile specimens. The specimens are subjected to uniaxial tensile load at one end and other end is fixed. In the present cases, the unit displacement (δl) as a tensile load along *x* axis is applied at one end. Then finite element simulations are carried out on the three tensile models. The strain energies for three cases are taken from the finite element simulations. The total strain energy of the tensile specimen in which the fibers are along the *x*-axis is 271.68 N-mm. 462.06 N-mm is the strain energy for the case where the fibers oriented along the *y*-axis. The strain energy of the specimen for the last case is 213.72 N-mm. The elemental strain energy contour plots for the three cases are shown in Fig.4. The elastic moduli are calculated by inserting strain energies in the equations 5, 6 and 8, and are presented in the Table 1.

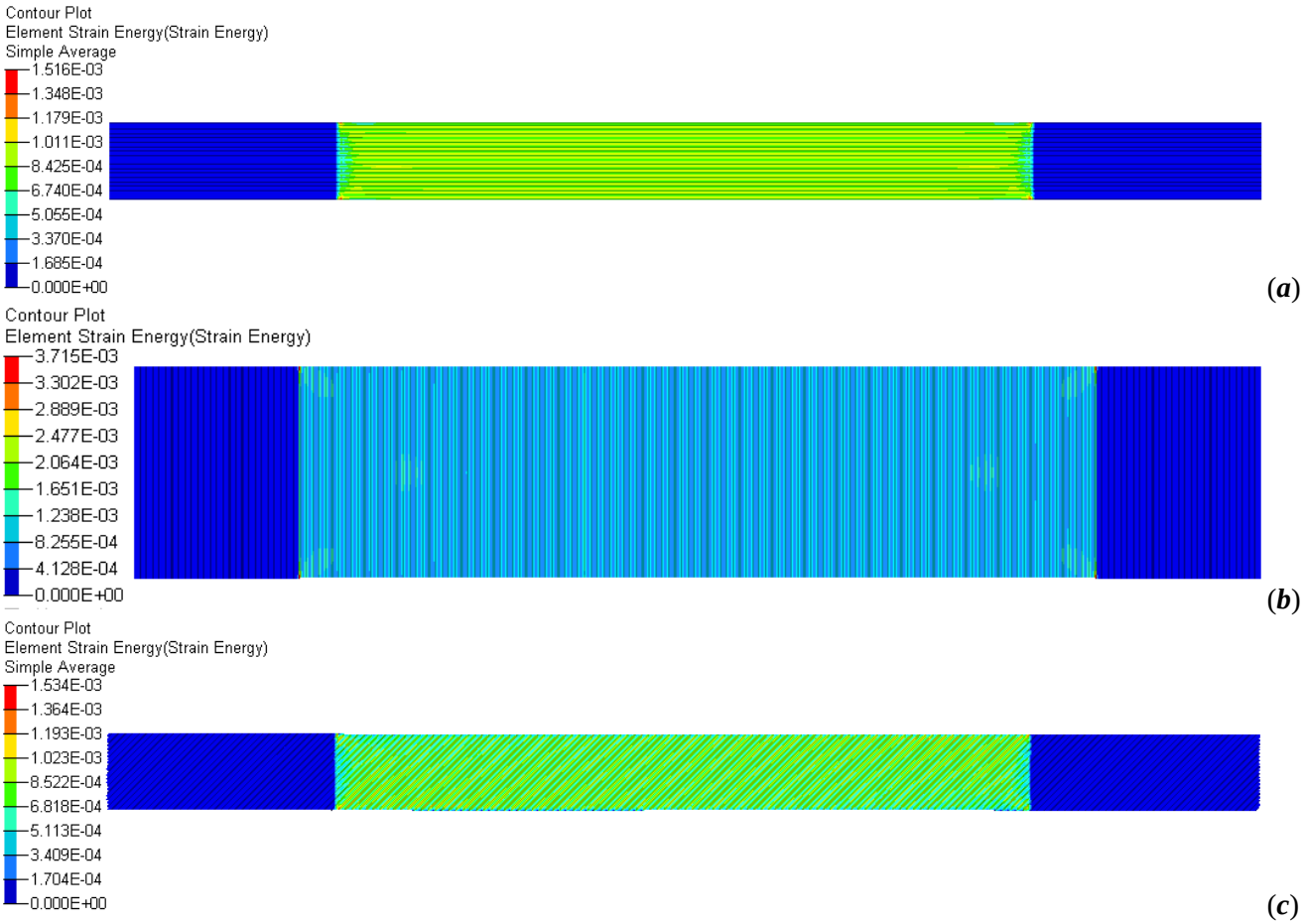

Figure 4. Strain energy plots of the uniaxial tensile specimens (a) fibers oriented along the load (b) fibers oriented transverse to the load (c) fibers off axis to load

The mesostructures of the printed parts using Stratasys µ print plus printer for two different cases are shown in Fig.3. Similarly, a mesostructure with a layer height of 0.254 mm is replicated in the FE models of the tensile specimens and then simulations are carried out to calculate the elastic moduli for this case. The elastic moduli for this case are presented in the Table.1. The present numerical results are compared with existing experimental results. The difference between the experimental and present results could be due to the variance in mesostructures present in the experimental tensile coupons by the researchers. However, the present numerical results are comparable with results of the experiments. The elastic moduli for layer thickness 0.330 and 0.254 are nearly same. This means that the layer thickness on elastic moduli is not greatly influenced in the present analysis. However, the elastic moduli in direction 2 could be improved if the layer thickness is further reduced. The reason for this is because the volume of the void areas between the adjacent roads would be reduced.

Table 1. Lamina properties of the FDM processed part

Elastic Moduli	Experimental			Present Numerical	
	Li et al [17]	Rodriguez et al [9]	Ziemain et al [24]	t =0.330 mm	t= 0.254 mm
E_{11}, MPa	2030.9	1972	1820.5	2205.1	2205.7
E_{22}, MPa	1251.6	1762	1103.2	1456.3	1485.4
ν_{12}	0.34	0.37	-	0.34	0.34
G_{12}, MPa	410.0	676	-	673.9	651.1

The elastic moduli of a layer obtained from the previous section would be useful in the constitutive matrix of a lamina for the analysis of laminated composite parts. In the next section, the elastic moduli are used in the characterization of the flexural behavior of the 3D printed parts using classical laminate theory.

Classical laminate theory for flexural behavior study: Analytical

In FDM, the filament is melted in the extruder and the molten liquid is pushed through the nozzle to deposit on the substrate in the *x-y* plane. Then the molten material on the substrate cools and solidifies into what is referred as 'road'. Depositing a number of roads side by side forms a single layer. Several layers together act as a laminate. Such fabricated parts are considered as unidirectional fiber reinforced laminates. A two-layer plate fabricated with FDM process with an orientation of the roads in layer 1 and 2 at 0° and 90° to *x*-axis of the plate, respectively is shown in Fig. 3.

The process parameters of the FDM influence the mechanical properties of the printed part. The raster orientation while depositing molten material in each layer can be defined by the user. Different orientations of road in layers lead to anisotropy in the properties of the printed parts. Process parameters such as the gap between two adjacent roads and the percentage of infill while printing governs the strength of the part. The internal architecture of a part fabricated using FDM is not significantly different from that of fiber reinforced laminate structure. Therefore, the laminate theory for analysis of composite laminate can also be used for analysis of FDM parts. The FDM processed parts resemble laminate structures and therefore these parts can be characterized with classical laminate theory. The constitutive relation for a lamina is available in Eq.8 and is rewritten here

$$\begin{Bmatrix}\sigma_{11}\\ \sigma_{22}\\ \tau_{12}\end{Bmatrix}=\begin{bmatrix}Q_{11} & Q_{12} & 0\\ Q_{12} & Q_{22} & 0\\ 0 & 0 & Q_{66}\end{bmatrix}\begin{Bmatrix}\varepsilon_{11}\\ \varepsilon_{22}\\ \gamma_{12}\end{Bmatrix} \tag{9}$$

The global coordinate system (*x,y,z*) for a laminate plate and local coordinate system (*1,2,3*) for a lamina are considered. Strains of the laminate from classical laminate theory is written as

$$\begin{Bmatrix}\varepsilon_{xx}\\ \varepsilon_{yy}\\ \gamma_{xy}\end{Bmatrix}=\begin{Bmatrix}\varepsilon^0_{xx}\\ \varepsilon^0_{yy}\\ \gamma^0_{xy}\end{Bmatrix}+z\begin{Bmatrix}k_{xx}\\ k_{yy}\\ k_{xy}\end{Bmatrix}, \qquad \{\varepsilon\}=\{\varepsilon^0\}+z\{k\} \tag{10}$$

where ε^0_{xx} and ε^0_{yy} are mid-plane strains in the laminate; γ^0_{xy} is the mid-plane shear strain in the laminate; k_{xx} and k_{yy} are bending curvature in the laminate; k_{xy} is the twisting curvature in the laminate and *z* is the distance from the mid plane in the thickness direction.

The constitutive relation for a laminate is written as

$$\begin{Bmatrix}\sigma_{xx}\\ \sigma_{yy}\\ \tau_{xy}\end{Bmatrix}=\begin{bmatrix}\overline{Q}_{11} & \overline{Q}_{12} & 0\\ \overline{Q}_{12} & \overline{Q}_{22} & 0\\ 0 & 0 & \overline{Q}_{66}\end{bmatrix}\begin{Bmatrix}\varepsilon_{xx}\\ \varepsilon_{yy}\\ \gamma_{xy}\end{Bmatrix}, \qquad \{\sigma\}=\left[\overline{Q}\right]\{\varepsilon\} \tag{11}$$

where $\overline{Q}_{ij}$ are transformed material constants, the elements of $\overline{Q}_{ij}$ are given as

$$\left[\overline{Q}\right]=[T]^{-1}[Q][T]^{-T} \tag{12}$$

where $[T]$ is a transformation matrix, T is given as

$$[T]=\begin{bmatrix}\mathrm{c}^2 & s^2 & 2cs\\ s^2 & c^2 & -2sc\\ -cs & cs & c^2-s^2\end{bmatrix} \tag{13}$$

where *c* is $\cos\theta$ and *s* is $\sin\theta$ and θ is the fiber orientation in anticlockwise direction to the *x*-axis.

The resultant force and moment per unit width for a laminate with N number of layers are expressed as

$$\begin{Bmatrix} N_{xx} \\ N_{yy} \\ N_{xy} \end{Bmatrix} = \int_{-h/2}^{h/2} \begin{Bmatrix} \sigma_{xx} \\ \sigma_{yy} \\ \tau_{xy} \end{Bmatrix} dz = \sum_{k=1}^{N} \int_{h_k}^{h_{k+1}} \begin{Bmatrix} \sigma_{xx} \\ \sigma_{yy} \\ \tau_{xy} \end{Bmatrix}_k dz \,,\ \{N\} = \sum_{k=1}^{N} \int_{h_k}^{h_{k+1}} \{\sigma\} dz \tag{14}$$

$$\begin{Bmatrix} M_{xx} \\ M_{yy} \\ M_{xy} \end{Bmatrix} = \int_{-h/2}^{h/2} \begin{Bmatrix} \sigma_{xx} \\ \sigma_{yy} \\ \tau_{xy} \end{Bmatrix} z\, dz = \sum_{k=1}^{N} \int_{h_k}^{h_{k+1}} \begin{Bmatrix} \sigma_{xx} \\ \sigma_{yy} \\ \tau_{xy} \end{Bmatrix}_k z\, dz \,, \qquad \{M\} = \sum_{k=1}^{N} \int_{h_k}^{h_{k+1}} \{\sigma\} z\, dz \tag{15}$$

Using Eq.10 and 11, and Eq. 14 and 15 become

$$\{N\} = \sum_{k=1}^{N} \left[\overline{\boldsymbol{Q}}\right] \left[\int_{h_k}^{h_{k+1}} \{\varepsilon^0\} dz + \int_{h_k}^{h_{k+1}} \{k\} z\, dz \right] \tag{16}$$

$$\{N\} = [\boldsymbol{A}]\{\varepsilon^0\} + [\boldsymbol{B}]\{k\} \tag{17}$$

$$\{M\} = \sum_{k=1}^{N} \left[\overline{\boldsymbol{Q}}\right] \left[\int_{h_k}^{h_{k+1}} \{\varepsilon^0\} z\, dz + \int_{h_k}^{h_{k+1}} \{k\} z^2 dz \right] \tag{18}$$

$$\{M\} = [\boldsymbol{B}]\{\varepsilon^0\} + [\boldsymbol{D}]\{k\} \tag{19}$$

where N_{xx} and N_{yy} represent the normal forces in the x and y directions (per unit width); N_{xy} is shear force; M_{xx} and M_{yy} denote the bending moments in the yz and xz planes; M_{xy} is the twisting moment; [***A***], [***B***] and [***D***] are the extensional stiffness matrix, coupling stiffness matrix and bending stiffness matrix for the laminate, respectively. The matrices [***A***], [***B***], [***D***] are functions of each lamina stiffness matrix [***Q***] and the distance from mid plane of the laminate to the laminas.

The mid-plane strains and curvatures can be calculated from Eq. 17 and 19, once we know the normal force and moment acting on a lamina. A symmetric laminate layup will have identical plies (including material, thickness and orientation) located at an equal distance above and below midplane of the laminate. For a symmetric laminate coupling matrix, [***B***]=[*0*] and therefore there is no extension-bending coupling. Therefore, the strains for a symmetric laminate subjected to only transverse loads are given from Eq.17 as

$$\begin{Bmatrix} k_{xx} \\ k_{yy} \\ k_{xy} \end{Bmatrix} = [D]^{-1} \begin{Bmatrix} M_{xx} \\ M_{yy} \\ M_{xy} \end{Bmatrix} \tag{20}$$

In the 3-point bending test, the load is applied in the z direction and for laminate thickness h, $M_{xx} \neq 0$, M_{yy}=0 and M_{xy}=0. The relationship between flexural stress and stiffness is written as $E_x^f = \sigma_{xx}^f / \varepsilon_{xx}^f$, using these above relations the flexural modulus of elasticity of the laminate along the x direction is given as follows

$$E_x^f = \frac{12}{[D^{-1}]_{11} h^3} \tag{21}$$

For instance, if the E_x^f of the laminate is calculated from Eq. 21, it is required to have the lamina's elastic moduli such as E_1, E_2, G_{12}, ν_{12}. These constants are found from the FE simulation of tensile testing mentioned above. Using these constants, the matrix [***D***] can be obtained, and then E_x^f of the laminate calculated using Eq. 21. To validate the calculated E_x^f of the laminate, experimental work is carried out to find E_x^f from the load versus

deflection curve of the bending test. The flexural stiffness of four different lamina layups is calculated using Eq. 21 and are presented in Table 3.

Flexural analysis of printed laminates: Experimental

This section describes about the flexural behavior of the printed laminates. The influence of fiber orientation and fiber thickness on the flexural stiffness is also studied using 3-point bending test. The FDM processed parts behave as a composite laminate structure, therefore mechanics of the composite laminates can be employed in their analysis. The flexural strength and stiffness of the laminate depends on several factors such as fiber orientation and type of lamina layup. Therefore, the influence of such factors on the flexural stiffness of the laminates should be investigated. The delamination, one of the major failure mode, in the laminates is due to bending loads. Therefore, it is important to study the flexural characteristics of the FDM processed parts for reliable design. In the present experimental investigation, a 3-point bending test, ASTM D7264 standard for the composite laminates is considered. The dimensions of the bending test specimen are shown in the Fig. 5. All dimensions of the specimen are presented in millimeters. To perform the test, the specimen is placed on two supports and then quasi-static transverse load is applied to the testing coupon at the center, as shown in the Fig. 5.

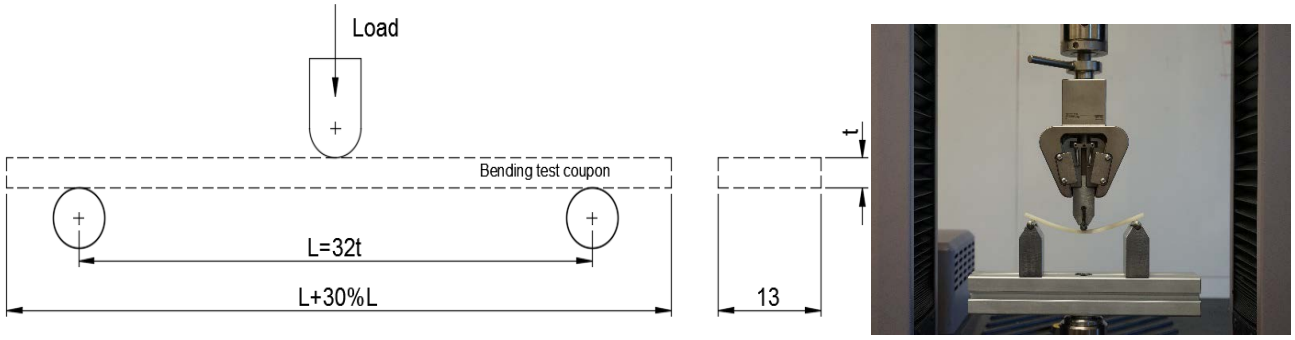

Figure 5. Bending testing of printed laminate and its dimensions

The specimens are printed using ABS-P430 supplied by the machine supplier and are built on a Stratasys µ print plus with default process parameters. Here, four different lamina layup are considered for two different cases. The layer size is different in both cases; 0.330 mm is the layer height in case *a* and 0.254 mm in case *b*. The dimensions of the printed laminates are available in Table 2. For each lamina layup, six samples are printed on a FDM machine that means 24 for each case. The orientation of fiber in four different laminates are provided in Table 3. Then, bending test are conducted on all specimens. The load versus deflection curves obtained from the tests are provided in the Fig.6 for case *a* and Fig.7 for the case *b*. The flexural stiffness (E_x^f) and its standard deviation (*SD*) are calculated using standard equations available in the ASTM D7264 standard. The experimental results for the case *a* and case *b* are provided in the Table 4 and 5, respectively.

Table 2. Printed laminate dimensions

	Fiber size, mm	Laminate thickness (t), mm	Number of layers	Span length, mm
Case. *a*	0.330	4.3	13	137.6
Case. *b*	0.254	4.3	17	137.6

Table 3. Elastic constants of a layer and symmetric lamina layup of the tensile specimen

	Elastic moduli of a layer for **Case. *a*,**	Elastic moduli of a layer for **Case. *b***

	E_1=2205.1 MPa, E_2=1456.3 MPa, ν_{12}=0.34, G_{12}=673.9 MPa	E_1=2205.7 MPa, E_2=1485.4 MPa, ν_{12}=0.34, G_{12}=651.6 MPa
Layup 1	[0°,90°,0°,90°,0°,90°,$\overline{0}$°]$_S$	[0°,90°,0°,90°,0°,90°,0°,90°$\overline{0}$°]$_S$
Layup 2	[15°,-75°,15°,-75°,15°,-75°,$\overline{15}$°]$_S$	[15°,-75°,15°,-75°,15°,-75°,15°,-75°,$\overline{15}$°]$_S$
Layup 3	[30°,-60°,30°,-60°,30°,-60°,$\overline{30}$°]$_S$	[30°,-60°,30°,-60°,30°,-60°,30°,-60°,$\overline{30}$°]$_S$
Layup 4	[45°,-45°,45°,-45°,45°,-45°,$\overline{45}$°]$_S$	[45°,-45°,45°,-45°,45°,-45°,45°,-45°,$\overline{45}$°]$_S$

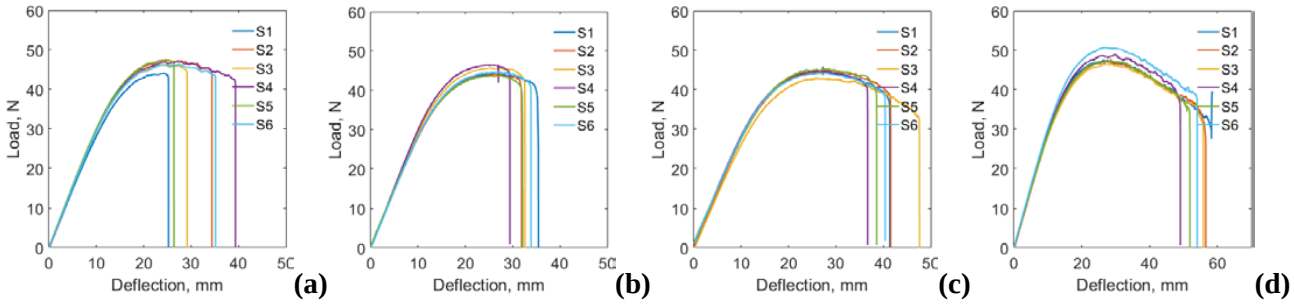

Figure 6. Load-deflection curves for a thick layer laminates (*a*) Layup 1, (*b*) Layup 2, (*c*) Layup 3, (*d*) Layup 4.

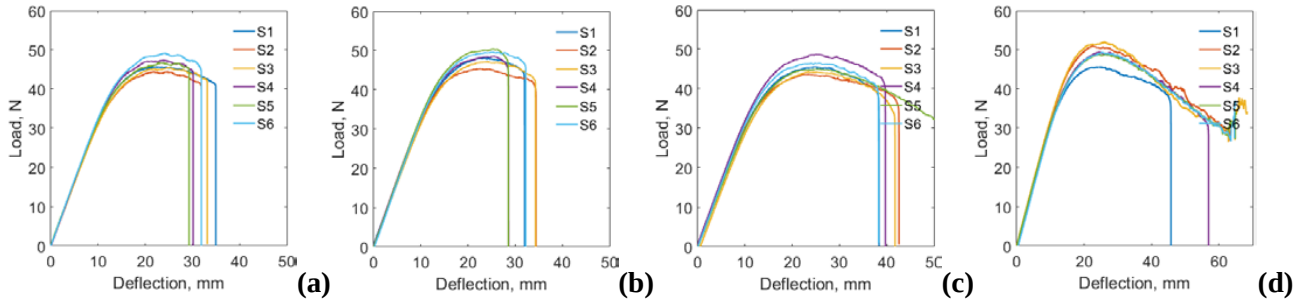

Figure 7. Load-deflection curves for a thin layer laminates (*a*) Layup 1, (*b*) Layup 2, (*c*) Layup 3, (*d*) Layup 4.

Thinner layer laminates have higher loading capacity when compared to thick layer laminates. Furthermore, these thinner layer laminates possess higher flexural stiffness than that of thick layer laminates. However, both thick and thin layer laminates have nearly same maximum deflection. This shows that the thickness of the fiber/road size or layer height influences the flexural stiffness, loading bearing and deflection of the laminate. The printing direction/fiber orientation of a lamina in the laminate also affected its flexural behavior. The flexural stiffness of the four different lamina layups calculated from CLT and experiments are provided for thick and thin layer laminates in the Tables 4 and 5, respectively. The flexural stiffness is higher for the case of layup 4 and lower for the layup 1 of laminate. Also, the layup 4 is undergone more deflection before failure when compare to the layup 1. For the thin layer laminates, some of the test coupon of the layup 4 laminates are not failed even at higher deflection. The flexural stiffness of the layup 4 type laminates is higher for the printed parts in contrast to the stiffness calculated using the classical laminate theory. The trend of stiffness of the laminate layup 1 to 3 calculated from experiments and CLT is decreasing, but for the laminate layup 4 is higher for the printed parts compared to the CLT results.

Table 4. Flexural modulus of elasticity of the laminate from classical laminate theory for thick layers

E^f_x, MPa	Analytical, CLT	Experimental ±*SD*	Difference, %
Layup 1	1923.1	1942.3±32	0.98
Layup 2	1888.5	1867.9±53	-1.10
Layup 3	1814.7	1779.4±40	-1.98
Layup 4	1754.5	1903.5±42	7.82

Table 5. Flexural modulus of elasticity of the laminate from classical laminate theory for thin layers

E^f_x , MPa	Analytical, CLT	Experimental ±*SD*	Difference, %
Layup 1	1914.9	2074.0±34	7.67
Layup 2	1870.6	2013.5±43	7.09
Layup 3	1782.0	1997.8±40	10.8
Layup 4	1723.2	2069.8±29	16.7

Failure analysis of 3D printed coupons under bending load:

The failure phenomena observed in the printed laminates is the fiber breaking and debonding of adjacent fibers. A laminate subjected to pure bending load and its crack surface are shown in the Fig.8. Failure mode in the laminate is ductile failure and the laminate layup 4 has higher ductility when compared to the laminate layup 1. The fiber breakage seen in a lamina, in which fibers are oriented at angle or along the *x*-axis and debonding is also seen in subsequent lamina, in which fibers are printed perpendicular to the orientation of fibers in previous lamina. Therefore, the crack surface is perpendicular to the fibers in the top or bottom surface layer of a symmetric laminate. The failure surface of a cross ply laminate is shown in Fig.8c. The layers of a laminate subjected to pure bending load and undergo tensile stress, if they are below the mid-plane and compressive load if they are above the mid plane. The load distribution in the fibers of a cross ply laminate is shown in Fig 8b., the fibers in bottom layers subjected to tension (T) and the fibers on top surface subjected to compressive (C) load. In case of the laminate layup 4, the fiber breaking is seen in all layers of the laminate. This is because the fibers in each lamina are subjected to same quantity of load, where as in other lamina layups the fibers oriented in layers along or at an angle to the length of the test coupon are subjected to higher tension load and the fibers in the subsequent layer the same laminate are subject to lower tension.

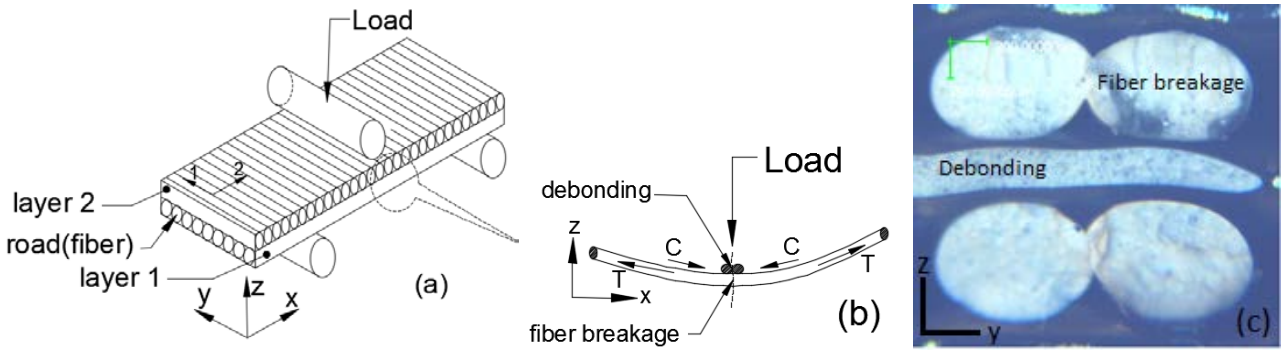

Figure 8. Printed laminate subjected to three point bending load (*a*) 0°/90° laminate (*b*) load on the fibers in a laminate (*c*) failure surface of cross ply laminate.

Conclusion

The parts fabricated via FDM processes are treated as laminated composite structures. The mechanics of laminated composites are adopted for the chracterization of mechanical behavior of the parts. The finite element procedure is presented to calculate the elastic moduli of a lamina of a printed laminated via FDM. The elastic moduli are used in the stiffness matrix for calculating the flexural stiffness of a printed laminate using classical laminate theory. Then the laminates of four different lamina layup with different layer thickness are printed. The effect of layer thickness and layup/printing oreintation on the flexural bhavior is investigated nummerically and experiemtnally. Thin layer printed laminates have maximum load bearing capacity and also higher energy absorption when compare to that of thick layer laminates. The FE procedure presented in this study can be used to find stiffness matrix of a printed lamina. Furthermore, it is confirmed with the experimental results that the

classical lamiante theory can be adopted for the characterization of mechanical behavior of the FDM printed laminates.

References

[1] Bourell, D.L., 2016. Perspectives on Additive Manufacturing. *Annual Review of Materials Research*, *46*, pp.1-18.

[2] Guo, N. and Leu, M.C., 2013. Additive manufacturing: technology, applications and research needs. *Frontiers of Mechanical Engineering*, *8*(3), pp.215-243.

[3] Wang, X., Jiang, M., Zhou, Z., Gou, J. and Hui, D., 2017. 3D printing of polymer matrix composites: A review and prospective. *Composites Part B: Engineering*, *110*, pp.442-458.

[4] General Electric report 2016, http://www.ge.com/ar2016/assets/pdf/GE_AR16.pdf

[5] Kotlinski, J., 2014. Mechanical properties of commercial rapid prototyping materials. *Rapid Prototyping Journal*, *20*(6), pp.499-510.

[6] Ahn, S.H., Montero, M., Odell, D., Roundy, S. and Wright, P.K., 2002. Anisotropic material properties of fused deposition modeling ABS. *Rapid prototyping journal*, *8*(4), pp.248-257.

[7] Bellini, A. and Güçeri, S., 2003. Mechanical characterization of parts fabricated using fused deposition modeling. *Rapid Prototyping Journal*, *9*(4), pp.252-264.

[8] Durgun, I. and Ertan, R., 2014. Experimental investigation of FDM process for improvement of mechanical properties and production cost. *Rapid Prototyping Journal*, *20*(3), pp.228-235.

[9] Rodríguez, J.F., Thomas, J.P. and Renaud, J.E., 2001. Mechanical behavior of acrylonitrile butadiene styrene (ABS) fused deposition materials. Experimental investigation. *Rapid Prototyping Journal*, *7*(3), pp.148-158.

[10] Tymrak, B.M., Kreiger, M. and Pearce, J.M., 2014. Mechanical properties of components fabricated with open-source 3-D printers under realistic environmental conditions. *Materials & Design*, *58*, pp.242-246.

[11] Dawoud, M., Taha, I. and Ebeid, S.J., 2016. Mechanical behaviour of ABS: An experimental study using FDM and injection moulding techniques. *Journal of Manufacturing Processes*, *21*, pp.39-45.

[12] Domingo-Espin, M., Puigoriol-Forcada, J.M., Garcia-Granada, A.A., Llumà, J., Borros, S. and Reyes, G., 2015. Mechanical property characterization and simulation of fused deposition modeling Polycarbonate parts. *Materials & Design*, *83*, pp.670-677.

[13] Bellehumeur, C., Li, L., Sun, Q. and Gu, P., 2004. Modeling of bond formation between polymer filaments in the fused deposition modeling process. *Journal of Manufacturing Processes*, *6*(2), pp.170-178.

[14] Zhou, X., Hsieh, S.J. and Sun, Y., 2017. Experimental and numerical investigation of the thermal behaviour of polylactic acid during the fused deposition process. *Virtual and Physical Prototyping*, pp.1-13.

[15] Coogan, T.J. and Kazmer, D.O., 2017. Bond and part strength in fused deposition modeling. *Rapid Prototyping Journal*, *23*(2).

[16] Kulkarni, P. and Dutta, D., 1999. Deposition strategies and resulting part stiffnesses in fused deposition modeling. *Journal of manufacturing science and engineering*, *121*(1), pp.93-103.

[17] Li, L., Sun, Q., Bellehumeur, C. and Gu, P., 2002. Composite modeling and analysis for fabrication of FDM prototypes with locally controlled properties. *journal of Manufacturing Processes*, *4*(2), pp.129-141.

[18] Casavola, C., Cazzato, A., Moramarco, V. and Pappalettere, C., 2016. Orthotropic mechanical properties of fused deposition modelling parts described by classical laminate theory. *Materials & Design*, *90*, pp.453-458.

[19] Alaimo, G., Marconi, S., Costato, L. and Auricchio, F., 2017. Influence of meso-structure and chemical composition on FDM 3D-printed parts. *Composites Part B: Engineering*, *113*, pp.371-380.

[20] Singh, R., Singh, S. and Fraternali, F., 2016. Development of in-house composite wire based feed stock filaments of fused deposition modelling for wear-resistant materials and structures. *Composites Part B: Engineering*, *98*, pp.244-249.

[21] Shofner, M.L., Lozano, K., Rodríguez-Macías, F.J. and Barrera, E.V., 2003. Nanofiber-reinforced polymers prepared by fused deposition modeling. *Journal of applied polymer science*, *89*(11), pp.3081-3090.

[22] Ning, F., Cong, W., Qiu, J., Wei, J. and Wang, S., 2015. Additive manufacturing of carbon fiber reinforced thermoplastic composites using fused deposition modeling. *Composites Part B: Engineering*, *80*, pp.369-378.

[23] Ziemian, C., Sharma, M. and Ziemian, S., 2012. *Anisotropic mechanical properties of ABS parts fabricated by fused deposition modelling*. INTECH Open Access Publisher.

[24] Ziemian, C.W., Ziemian, R.D. and Haile, K.V., 2016. Characterization of stiffness degradation caused by fatigue damage of additive manufactured parts. *Materials & Design*, *109*, pp.209-218.

[25] Hart, K.R. and Wetzel, E.D., 2017. Fracture behavior of additively manufactured acrylonitrile butadiene styrene (ABS) materials. *Engineering Fracture Mechanics*.

[26] Tekinalp, H.L., Kunc, V., Velez-Garcia, G.M., Duty, C.E., Love, L.J., Naskar, A.K., Blue, C.A. and Ozcan, S., 2014. Highly oriented carbon fiber–polymer composites via additive manufacturing. *Composites Science and Technology*, *105*, pp.144-150.

[27] Jones, R.M., 1998. *Mechanics of composite materials*. CRC press.